# DESIGN OF AN APPARATUS TO DETECT SMALL CHANGES IN THE MASS OF ROTATIONAL MACHINE COMPONENTS

Jonathan R. A. Maier, Clemson University; M. Laine Mears, Clemson University; Joshua D. Summers, Clemson University

## Abstract

In this study, an apparatus was designed to detect changes on the order of grams in the mass of test samples subject to accelerations approaching 275g. The apparatus incorporated a surface speedometer, displacement transducer and on-board data-logging device in order to correlate mass loss events with changes in rotational speed and acceleration. An accessory was also designed to allow for on-board video recording to validate the findings and to better understand the mechanics of mass loss events. Such mass loss events are of interest for high-speed rotating machinery (e.g., manufacturing equipment, turbine rotors and automotive drivetrains), where material can build up and be dislodged, or other mass loss events can occur that currently cannot be measured directly. Results of such a design will allow for identification of mass loss in service for improved equipment diagnostics and control.

## Motivation: Measurement of Mass Loss Events in Rotating Machinery

### Mitigation of Safety Risks

Rotating machinery, including industrial machines, automobiles, aircraft turbines, etc., pose a serious safety hazard. According to the U.S. Department of Labor Bureau of Labor Statistics, 458 people were killed in the United States by machinery in the year 2005. This is 8% of the 5,743 total fatal occupational injuries for that year. Of the 458 deaths involving machinery, 105 involved some kind of rotating machinery [1]. Meanwhile, the National Highway Traffic Safety Administration (NHTSA) estimates that about 400 fatalities were the result of tire failures between the years 1994 and 2004, or an average of about 40 tire-failure-related deaths per year [2]. The Bureau of Labor Statistics also reports that between the years 1995 and 2002, 459 people were killed in helicopter-related incidents. About 2% of these deaths involved the decedent being struck by the rotating helicopter blades [3]. Loss of turbine blades in aircraft engines is an additional source of fatalities. For example, flight GA865 in 1996 aborted its take-off attempt after a turbine blade separated from one of the three engines. The resulting crash killed 3 of the 260 passengers on-board [4].

High-speed rotating machinery is commonplace in manufacturing, power generation and transportation. The high rotational speeds induce high centripetal acceleration, particularly at larger radii. As the centripetal acceleration increases with speed, so does the force necessary to hold anything attached to the equipment. Failure to retain screws, rivets, coatings or, in particular, debris can lead to rotational imbalance and equipment failure. Moreover, the loss of objects at speed poses a safety risk from the projectile motion of the ejecta.

### Difficulties in Measuring Mass Loss on Rotating Machinery

Observing rotating machinery from a fixed standpoint is difficult as the speed of rotating machinery quickly outpaces video speed and capabilities (e.g., trying to film the tips of helicopter blades), and protective enclosures often obscure a direct view of equipment. The observation of mass loss events from high-speed rotating machinery *in situ* is very difficult for a number of reasons. Detection equipment itself, if mounted to the rotating element, will tend to cause imbalance (such as sensors on a turbine blade) and, therefore, is difficult to attach safely to equipment. If detection equipment is attached, then data must be recorded on the rotating machine since wires cannot be connected to a stationary data logger without twisting the wires or introducing electrical noise and wear through a slip coupling. Wireless transmission is complicated by the electromagnetic effects induced by the rotation of antennae and large power sources typical of such equipment. On-board data logging cannot involve moving parts (such as a hard drive or tape heads) since the large centripetal accelerations would cause these parts to malfunction.

Fortunately, recent advances in data-logging capability, particularly involving solid-state memory, do not have any moving parts and, thus, are ideally suited for recording on-board a dynamically moving machine. A test apparatus was

designed that incorporated commercially available data-logging to solid-state memory, and a displacement transducer to record mass loss events. The apparatus provides for on-board data collection and video recording at much lower cost compared to conventional approaches to outfitting a machine in service.

The conventional approach to identifying failure is to measure vibrations in the stationary part of the machine (e.g., the mounts) and to correlate anomalies in the vibrations to some reference model or signature of "normal" operation. In this way, imbalances can be potentially detected and failures—such as a cracked shaft, parts rubbing, worn bearings, etc.—diagnosed. However, expert knowledge is needed to correlate vibration data with the various causes of mechanical failure [5]. Specifically, a challenge to identification techniques is the excitation of the rotating structure where it is not easy to access the rotor to measure the forces.

In response to the urgency of studying rotating machinery, and in light of the problems inherent in the conventional approach, the aim of this design was to produce a dedicated apparatus on which mass loss events on the order of single grams could be detected and recorded from individual parts affixed and spun at speeds sufficient to achieve centripetal accelerations on the order of hundreds of g's. The means for recording the resulting data are discussed in subsequent sections.

# Design Approach

A project sponsor presented the design team with the need for a machine capable of detecting mass loss events on the order of single grams at rotational accelerations of up to 274g. Additional constraints pertained to the accommodation of proprietary test samples, as well as the safety and location of the machine. Critical design constraints and criteria are shown in Table 1.

The design phase of the project lasted four months and included requirements evaluation, technology assessment and preliminary simulations, candidate design development, a Preliminary Design Review (PDR), detail design proposal with integrated subsystems, development of testing protocols and a Comprehensive Design Review (CDR). The fabrication phase of the project lasted another four months and included ordering components, fabricating the system, control design, programming and calibration procedures, initial functional testing and prototype demonstration to the project sponsor. The validation phase of the project lasted a final four months and included statistical Design of Experiments (DoE), validation testing using proprietary test samples, performance evaluation, repeatability and reproducibility characterization and training of operating personnel.

**Table 1. Design Constraints and Criteria**

| Constraints | Criteria |
|---|---|
| Test samples will have mass of 1.5 kg | Repeatability of tests |
| Test samples must be held at a radial distance of 0.4 meters | Ability to test different sample geometries |
| Mass loss events on the order of single grams must be detected | Ability to test samples under different physical conditions |
| Voids created in the sample by loss of mass on the order of single grams must be detected | Cost of machine |
| Maximum centripetal acceleration encountered by the samples must be 274g | Safety of machine operation |

Early in the design phase, free-body diagrams of the sample and mass loss events were drawn (see Figure 1). The free body diagram shows a hypothetical part before it is released from the rotating sample. The forces shown in the free body diagram act to hold the particle to the sample and to push it out of the sample. The forces acting to hold the particle in the sample (i.e., acting to the right in Figure 1) are chemical or mechanical bonding between the particle and sample, $F_{bonding}$, spring action from two or more sides if the particle is wedged, $F_{spring}$, friction force between the particle and the sample, $F_{friction}$, and suction created by any trapped air between the particle and the sample, $F_{air}$. The forces acting to push the particle out of the sample (i.e., acting to the left in Figure 1) are centrifugal effects, $F_{cent}$, punch from the sample flexing as it rotates, $F_{punch}$, and gravity when the sample is facing downward, $F_{gravity}$.

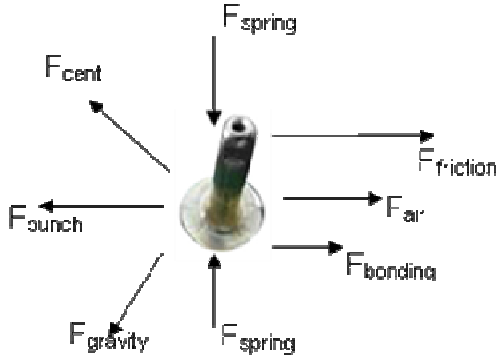


**Figure 1. Free-Body Diagram of Mass Events**

Continuing in the design phase, a systematic engineering design process was followed [6]. In particular, a high-level functional model of the prototype system was generated (see Figure 2), and system concepts were explored using a morphological matrix (see Table 2).

Feasible system concepts were discussed during the PDR leading to the selection of the final concept for prototype development. In particular, it was decided that the sample would be attached to the machine using a clamping assembly that would clamp on to geometrical features embedded in each sample. The sacrificial mass was to be loaded in discrete batches by hand. The rotational movement of the sample was to be accomplished through accelerating up through multiple rotations rather than a single rotation or by linear motion. The forces were to be measured directly using a displacement transducer as well as indirectly through video recording. Voids created in the sample as a result of testing were to be measured by weighing the sample before and after each test.

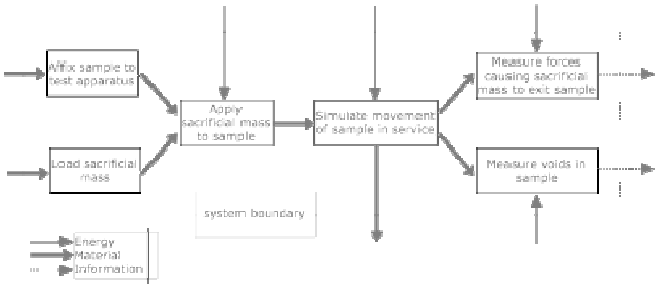


**Figure 2. System Functional Diagram**

Following the PDR, solid models were developed using computer-aided-design (CAD) software and the details of the prototype design were discussed at the CDR prior to prototype fabrication and validation. Details of various aspects of the prototype are described in subsequent sections, including how data displacement transducer data and video data are recorded on board the rotating machine, the primary sensing strategy involving the displacement transducer and additional sensing capabilities, the control strategy for achieving specific rotational speeds, and how the rotating machine is balanced.

**Table 2. Morphological Matrix. Shaded Concepts Were Chosen for Prototype Development**

| **Functions** | **Solution Concepts** | | | | | | | | |
|---|---|---|---|---|---|---|---|---|---|
| Affix sample to test apparatus | Apply normal force to top | Radially | Clamps | Adhesives | Screws / bolts | Suction pressure | Strings / Rubber bands / straps | Embedded feature in sample | Magnetic |
| Load sacrificial mass | Pan (discrete) | In a track / conveyor (continuous) | In a bottle | | | | | | |
| Apply sacrificial mass to sample | Raise pan vertically | Conveyor belt | Spray | Move pan horizontally | Move sample vertically | Pack by hand | | | |
| Simulate movement of sample in service | Rotate sample through multiple rotations | Rotate sample through one rotation | Rotate sample through partial rotation | Radial or linear movement to impact a stop | Deflect sample by applying simulated road | Deflect sample directly with actuators | | | |
| Measure forces causing sacrificial mass to exit sample | Spring scales | Strain gauges / displacement transducers | Load cells / force transducers | Indirectly through measuring velocity optically / radar / ultrasonic / x-ray / etc. | Accelerometers | Rotary encoder | Sensors (nano) in sacrificial mass | Sensors (nano) in sample | Measure embedded traceable particles (metal / radioactive / etc.) |
| Measure voids in sample | Measure weight after packing and then after movement | Calculate void indirectly based on forces and density of sacrificial mass | Measure directly volume / height of mud between grooves | Directly through optically / radar / ultrasonic / x-ray / etc. | Measure traceable particles (metal / radioactive / etc.) embedded in mud and / or tire | | | | |

Similar prototype machine designs have recently been reported in the literature, including the design of a gripper with a spherical parallelogram mechanism [7], the design and prototyping of a partially decoupled 4-DOF 3T1R parallel manipulator with high-load carrying capacity [8], and the design of a microrobotic wrist for needle laparoscopic surgery [9]. Similar to the design of these mechanisms, the design of the apparatus to detect small changes in mass of machines at high rotational speeds described in this paper serves to fulfill a critical industrial need.

# System Overview

The system designed and built in this study is illustrated in Figure 3. This system generally is composed of a test-sample mounting fixture, a blast shield for personnel and equipment protection, a high-resolution camera for event visualization, a data logger and a motor-control system. The sensing and control systems were of particular interest in this study and are discussed in subsequent sections.

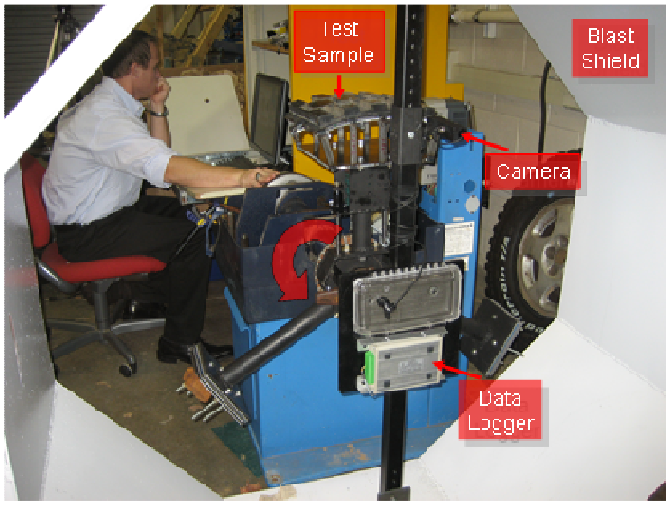


**Figure 3. System Physical Architecture**

The test sample fixture is a key mechanical element in this system (Figure 4).

The clamping assembly includes the surface on which samples may be placed from which a fly-off event will be measured. This clamping assembly is connected to a system of roller guides to allow for radial extension that is force controlled with an internal compression spring. Further, two balancing arms are included to ensure that the loads on the motor and shaft system are continuous. Dimensions for the system were redacted to adhere to the proprietary wishes of the sponsoring organization.

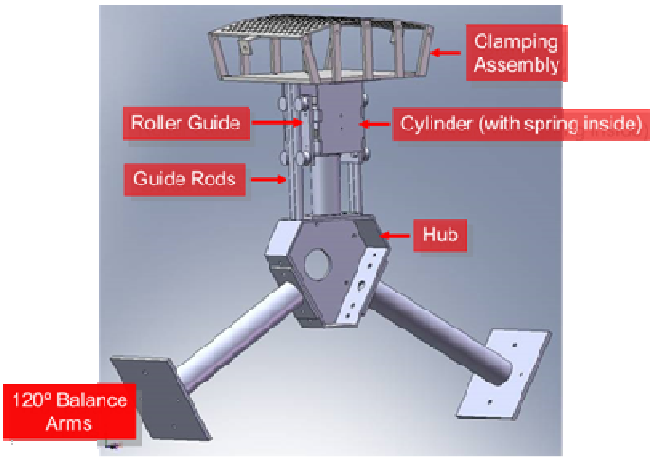


**Figure 4. Fixture Assembly**

The next section explains the data-logging challenges and solutions integrated into this system. The following section presents the video recording strategy employed. Finally, the sensing and control strategies necessary to realize this system are explained.

# Recording Data on a Rotating Machine

Data loggers such as hard disk drives and tape drives that rely on moving parts will fail in situations where they will suffer shock loading or the similar effects of hundreds of g's of centripetal acceleration. A recent finite element analysis of hard disk drives by Lin [10] found that accelerations as low as 260g's will cause physical damage at the interface between the rotating plates and the fixed sliders.

The advent of flash memory in the last decade has revolutionized memory storage on a wide range of platforms including cellular phones, digital cameras, hand-held computers and even household thermostats [11]. Robust yet inexpensive high-speed data loggers are now available which are capable of operating on low-voltage battery power and record onto standard flash memory cards. Such data loggers are immune to the effects of centripetal acceleration since they do not have any moving parts. Similar data loggers are now commonly used in environments where high-voltage power is not available and harsh conditions, such as for data logging on board race cars, are present. For the prototype machine, the Dataq DI-710 with data sampling speeds of up to 14.4 KHz and a high-speed Secure Digital flash memory card with 1 GB capacity was selected. The data logger was mounted near the center of the testing apparatus in order to minimize the forces on the mounting hardware and wire connections.

# Recording Video on a Rotating Machine

In addition to the ability to record mass loss events using the data logger described in the previous section, video recording can yield additional information relevant to the mechanics of how mass loss events occur. Frame-by-frame analysis can reveal the originating location and trajectory of ejecta and events precipitating mass loss, such as crack propagation or initial plastic failure of components. Video recorded on-board the rotating machinery enables superior image capture capability compared to video recorded from a stationary location, because the configuration is not as sensitive to sampling rate, and rotation of the machinery itself does not obscure the view of the component of interest, which appears fixed in the frame.

However, recording video data on board the rotating machine poses the same challenges as recording data from the displacement transducer—namely, the recording must be on solid-state memory (no moving parts) and must operate on low-voltage battery power. Whereas most video recorders, whether analog or digital, utilize magnetic tapes or hard disk drives, digital video recorders (DVRs) have recently been introduced that compress the video signal in real time and record onto solid-state flash memory. When paired with a fixed-lens digital CCD camera, the DVR system contains no moving parts and is well suited to video recording on board the rotating machine. This type of solid-state recording setup has found popularity with sporting enthusiasts, for example, in sturdy helmet cameras that can record "first person" action during motorcycle racing, open-cockpit auto racing, and even sky-diving, kayaking and skiing. These systems are robust enough to withstand not only the rigors of racing but also high-acceleration impact events such as crashes.

For the prototype machine in this study, a Sony bullet-style camera with 560-line resolution paired with a mini DVR that records at 320x240 resolution and 30 frames per second was chosen. Both the camera and DVR were mounted within protective enclosures. Both devices ran off of the same battery pack that powered the separate Dataq data logger.

# Sensing Strategies

## Primary Sensing Strategy

The machine was designed to detect changes in mass of a test sample while the sample rotates at speed. The on-board data logger discussed above provides a means for recording electrical signals. The choice was, therefore, for a transducer that would detect mass loss events and convert those events to an electrical signal for the data logger to record. The simplest concept for the apparatus was to have a rigid arm with a strain gauge attached that would be able to resolve changes in the axial deflection of the arm as individual mass loss events occur. However, the arm would have to be very thin in order to get significant strain for mass loss events on the order of single grams.

As noted in Table 1, the test sample under study had a mass of 1.5 kg, was held at a radial distance of 0.4 meters, and the machine had to detect a change in mass on the order of 1 gram at a maximum centripetal acceleration of 274g. The centrifugal force on the sample at maximum speed can be calculated as follows, taking 300g as a worst-case scenario rather than 274g:

$$a = F / m \tag{1}$$

$$300 \cdot 9.81 = F / 1.5 \tag{2}$$

$$F = 300 \cdot 9.81 \cdot 1.5 \tag{3}$$

$$F = 4414.5 \text{ N} \tag{4}$$

where the maximum radial speed is:

$$F = m \cdot \omega^2 \cdot r \tag{5}$$

$$4414.5 = 1.5 \cdot \omega^2 \cdot 0.4 \tag{6}$$

$$\omega^2 = 4414.5 / (1.5 \cdot 0.4) \tag{7}$$

$$\omega^2 = 7357.5 \tag{8}$$

$$\omega = 85.8 \text{ radians/second} \tag{9}$$

and the change in force for the loss of one gram is:

$$F = m \cdot \omega^2 \cdot r \tag{10}$$

$$F = 0.001 \cdot 85.8^2 \cdot 0.4 \tag{11}$$

$$F = 2.94 \text{ N} \tag{12}$$

A typical strain gauge will not detect changes in strain ε below 0.01%, or ε=0.0001. For aluminum, with a Young's modulus of $E = 69 \cdot 10^9$ N/m$^2$, the cross section of the arm, $A_{xc}$, can be calculated to detect events at maximum radial speed, ω:

$$\varepsilon = F / (A_{xc} \cdot E) \tag{13}$$

$$0.0001 = 2.94 / (A_{xc} \cdot 69 \cdot 10^{9}) \tag{14}$$

$$A_{xc} = 2.94 / (0.0001 \cdot 69 \cdot 10^{9}) \tag{15}$$

$$A_{xc} = 4.26 \cdot 10^{-7} \text{ m}^2 \tag{16}$$

$$A_{xc} = 0.426 \text{ mm}^2 \tag{17}$$

In order to support a strain gauge one centimeter wide, the arm would only be 0.04 mm thick, far too thin to be structurally feasible. To detect mass loss events at lower speeds would require the arm to be thinner still. The conclusion is that a strain gauge acting alone is not sensitive enough to detect mass loss events on the order of single grams.

Consequently, a spring system to mechanically amplify length changes was developed. A compression spring rather than an extension spring was selected for two reasons. First, compression springs are available with shorter lengths and higher stiffness (in particular, die springs) than available extension springs. Second, if the machine is overloaded, a compression spring will fully compress and then act as a rigid cylinder, whereas an extension spring would over extend and potentially fail.

An overview of the chosen sensing strategy is shown in Figure 5. A computer workstation controls a motor which accelerates the apparatus up to speed. The test sample is held on a compression spring. When mass loss events occur, the decrease in the sprung mass causes the centrifugal force on the spring to decrease; the compression spring then extends (on the order of millimeters for mass loss events on the order of grams). A linear potentiometer acts as a displacement transducer, converting changes in the piston length of the potentiometer into changes in electrical resistance. A separate battery back supplies DC voltage to the linear potentiometer. The data logger finally records the difference in voltage across the linear potentiometer over time.

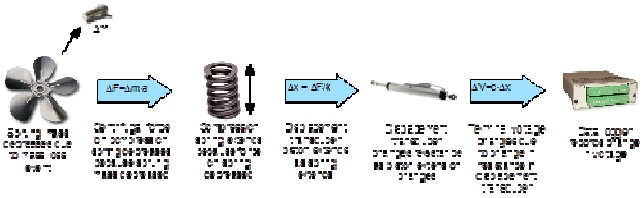

**Figure 5. Working Principles in the Apparatus**

The time at which events occurred can be extrapolated based on the sampling frequency set on the data logger. The rotational speed, and therefore centripetal acceleration, at which events occur can be inferred based on the speed profile supplied to the motor, or via a second speedometer channel recorded on the data logger. The use of recorded speedometer data is particularly helpful as the speed profile on the motor controller may not actually be achieved by the motor due to slip and friction losses. The data analysis can be performed in any commercially available analysis package such as Matlab, DaDisp or DIAdem.

# Spring Selection

The dimensions of the spring must match the capabilities of the displacement transducer; however, another important consideration is that the spring stiffness must exceed the natural frequency of the sprung load. The sprung load consists of not only the test sample, but also the clamping apparatus necessary to hold it. The combined mass of the sprung load in the prototype was approximately 9 kg. The frequency of the machine at maximum speed is:

$$f = \text{rotational speed (Hz)} = \text{rotational speed (radians/second)} / (2\pi \text{ radians/rotation}) \tag{18}$$

$$f = 85.8 / (2\pi) \tag{19}$$

$$f = 13.7 \text{ Hz} \tag{20}$$

The minimum stiffness of the spring can then be calculated:

$$f_n = 0.5\pi\sqrt{k/m} \tag{21}$$

$$2 \cdot f_n = k / (4\pi 2m) \tag{22}$$

$$k = 4\pi^2 f_n^2 m \tag{23}$$

$$k = 4\pi^2 \cdot (13.7 \text{ rot/sec})^2 \cdot 9 \text{ kg} \tag{24}$$

$$k = 66687 \text{ kg/sec}^2 \tag{25}$$

$$k = 66687 \text{ N/m} = 381 \text{ pounds/inch} \tag{26}$$

To be above the natural frequency of the machine running at top speed, the spring must be stiffer than 381 pounds/inch. In addition, the spring must be able to carry the sprung load at maximum speed:

$$F = m \cdot a \tag{27}$$

$$F = 9 \text{ kg} \cdot 300 \cdot 9.81 \text{ m/sec}^2 \tag{28}$$

$$F = 26487 \text{ N} = 5954 \text{ pounds} \tag{29}$$

The current spring in use in the machine has a maximum load of 2,000 pounds and a spring rate of 2,900 pounds/inch. The current spring was, therefore, 7.6 times the stiffness necessary to be above the natural frequency of the system; however, it was undersized by about two thirds relative to the maximum load at speed. In the current test setup, it was presumed that much of the mass (which was artificially added to the test sample) will have dislodged by maximum speed, such that the spring would not need to carry the whole 5,954 pounds of maximum load. Using an undersized spring with respect to maximum load allows for greater resolution at lower rotational speeds.

To match the chosen spring, which has a maximum deflection of 23% of 3 inches overall height, which is 0.69 inches or 1.75 cm, a displacement transducer with 2.5 cm stroke length was selected. A linear motion potentiometer was chosen because they have essentially unlimited resolution. The effective resolution is limited only by the data logger which, for the Dataq DI710, is 14 bits.

# Additional Sensing Capabilities

Besides the record of mass loss events captured on-board in the data logger, mass loss events can be detected by other means, both on-board and off-board the machine. On-board the machine, the video camera captures a video record of every particle that leaves the test sample within the field of view, within the resolution and frame rate capabilities of the camera. Off-board the machine, stationary video and audio capture is also possible, which is particularly effective in capturing the audible signature of ejecta hitting the safety shield, which is in place around the machine. Another means for detecting mass loss events is using the conventional approach, where sensors detect increasing vibration in the drive shaft. Sample data recorded using each sensing strategy are presented in the section on sample data.

## Control Strategy

An industrial three-phase motor turns the prototype. The motor is controlled by a Telemechanique Altivar 71 motor drive. The motor drive can be deactivated manually using a shut-off switch. The motor drive is itself controlled by a computer running LabVIEW software and a proprietary motor-control software. Different motor states are actuated using a set of hardware relays which are switched on and off by the LabVIEW software through a National Instruments USB-6009 DAQ interface. In addition to spinning the prototype, the motor is also connected to a quadrature encoder and to piezo-electric sensors. The quadrature encoder signal and piezo-electric sensor signals are inputted to LabVIEW through the DAQ interface.

The LabVIEW software running on the computer presents the user with real-time speed data based on the quadrature encoder signal. The speed data are also stored to a data file which may be accessed and viewed after the test to see the details of the actual speed and behavior of the motor. Examining the actual motor behavior is important because while the control software may be programmed for any arbitrary speed profile, the motor has physical limitations such that it may not be able to fully achieve programmed accelerations, decelerations and set speeds.

The ability of the user to see in real-time the rotational speed of the prototype is important because, for safety reasons, the operator may not be in the same room as the prototype during a test; that is, the computer and operator may be located remotely. Thus, via the speedometer reading, the LabVIEW software allows the user to know when the test starts and when it has come to an end. In the case that there was an initial setting that was set incorrectly and the motor does not behave as the user intended, it will also show this and the user will then be able to make the appropriate changes to conduct another test with corrected settings. Also located on the front panel were “start” and “stop” buttons for beginning and, if necessary, prematurely ending a test. The LabVIEW program was designed to shut itself off after conducting the appropriate functions for any given test.

Also located in the LabVIEW block diagram were the controls for the relays that control the starting, stopping and other speed changes of the motor. The time for which the relays will change the output of the motor was controlled from the front panel when LabVIEW is running and can be set in milliseconds. Each change in relay state can be programmed for a corresponding change in step-wise or ramp acceleration (or deceleration) of the motor.

# Balance Strategy

The sample was held at a radial distance from the center of the drive axle to increase the centripetal load. That load had to be balanced in order not to place large and potentially detrimental unbalancing forces on the machine which will ultimately cause fatigue and excessive vibration, both potential safety hazards.

Since mass will be lost from the sample during testing, unless the balance mass adjusts, the machine will have some amount of imbalance. In order to minimize complexity in the machine, a variable-balance mass was not integrated. Rather, two balance arms were placed at 120° from the in-

strumented arm, rather than one balance arm at 180° from the instrumented arm. The imbalance caused by mass loss events is thereby a smaller proportion with respect to two balance arms than it would be compared to a single balance arm.

The hub geometry necessary to accommodate one instrumented arm and two balance arms is fundamentally an equilateral triangle. However, in order to minimize the mass and stress risers of the hub, the three "points" of the triangle are truncated, resulting in a hexagonal design (Figure 6).

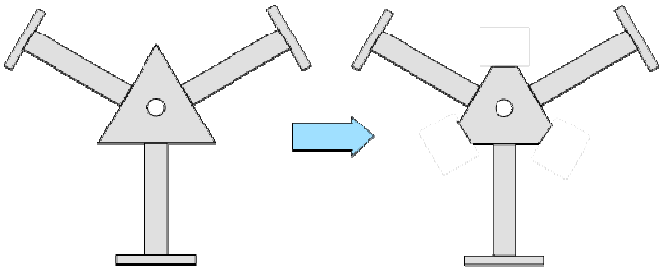

**Figure 6. Triangular Hub Design versus Hexagonal Hub Design**

Meanwhile, the video camera, which is held at a longer radial distance than the test sample, must also be balanced. Since the camera does not lose mass, it would not benefit from balance mass at 120°. Therefore the camera was held on a separate mount with balancing at 180°. The mount allows for the camera to move radially from 0.4 to 0.6 meters in order to provide for different video angles of the sample, from edge-on to nearly top-down showing the whole sample within the field of view. In the prototype, the data logger, digital video recorder and battery pack were mounted on a plate at the center of the camera arm. The finished prototype system is shown in Figure 7. The various components of the assembly shown in the images include the central hexagonal hub, balance arms, main cylinder with spring, roller guides and guide rods, and the clamping assembly holding the test sample. Note that the camera arm mounts to the central hexagonal hub. The physical prototype shown in Figure 7 is placed within a radially protective shield made of 6mm-thick steel.

# Analysis Strategies

## Analyzing Displacement Transducer Data

The principal challenge in the analysis of the data is to distinguish individual mass loss events. Ideally, mass loss events should appear as stepwise decreases in the displacement transducer data (highlighted by the red arrows in Figure 8).

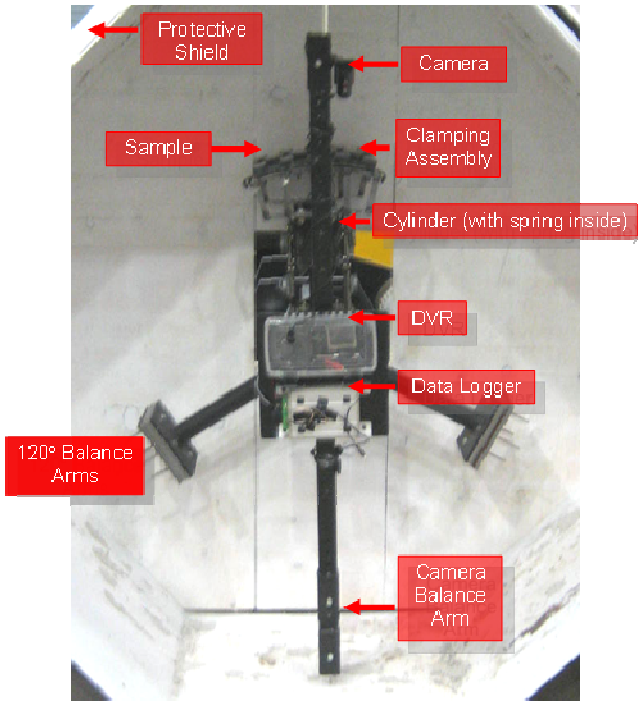


**Figure 7. Physical Prototype**

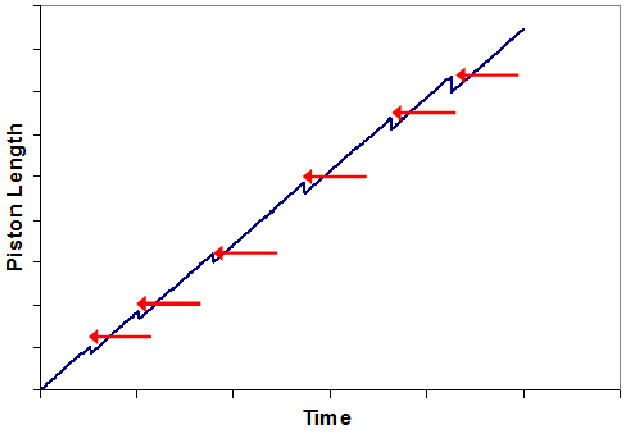


**Figure 8. Theoretical Plot Showing Piston Length of the Displacement Transducer Versus Time for a Ramp Input to the Motor. Mass Loss Events Appear as Down-Steps**

Several effects on the machine act to make the real data more noisy and mass loss events more difficult to distinguish. One such effect is gravity. Since the apparatus rotates in a vertical plane, directionality of the gravitational force affects the sensor readings. Fortunately, this is predictable at low speeds, and as the speed of the apparatus increases, the effect of the gravity force is proportionally smaller com-

pared to the centrifugal force. The effect of gravity can be removed from the data by calculating the gravity force and consequential displacement for the given rotation angle at any time. The angle of rotation is accurately synchronized with the angle at which the gravity force is calculated through the LabVIEW real-time engine.

Another effect is electrical noise. Since the data logger runs off battery power, which is not well conditioned, the signal through the displacement transducer exhibits noise, even when at rest (see Figure 9). The noise occurs at a higher frequency than either the gravity effect or the frequency of mass loss events, so the electrical noise can be effectively removed using a low-pass filter without significantly affecting sensing of mass loss events. Figure 10 shows the transducer data at rest filtered using a running average with n=398.

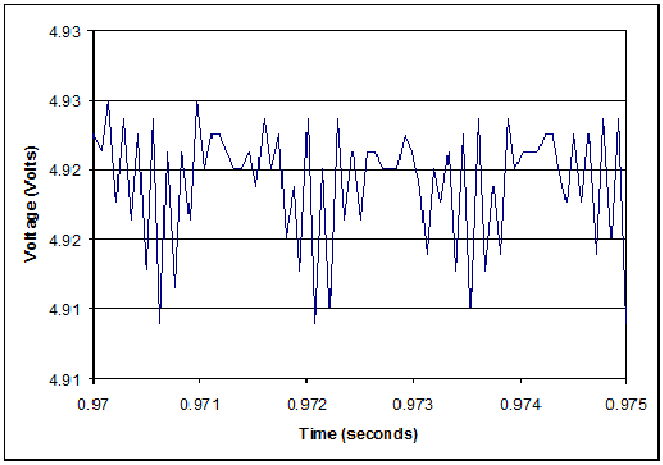


**Figure 9. Transducer Signal at Rest (Unfiltered)**

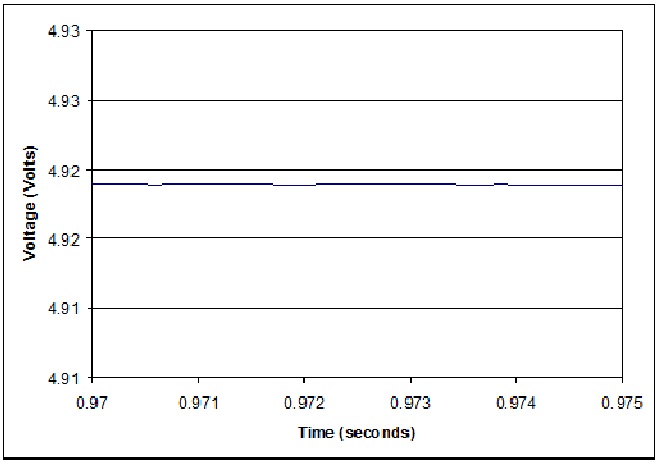


**Figure 10. Transducer Signal at Rest (Filtered)**

Friction and clearances in the moving components can also introduce noise into the data through excessive stick-slip phenomena. For this reason, precision roller guides were used in place of sliding linear guides, which helped to eliminate lateral movement and constrained the test sample more closely to move radially as the spring compressed and decompressed.

## Smallest Mass Loss Event Discernible using Primary Sensing Strategy

Using the primary sensing strategy of the analog displacement transducer connected to the digital 14-bit data logger, and a range of displacement of 1.75 cm, and taking into account the manufacturer's specification of the data logger of a noise floor of 2 bits, changes in displacement must result in a change of at least 3 bits. The smallest detectable change in length of the displacement transducer is therefore:

$$(1.75\ \text{cm}/2^{14}\ \text{bits})\cdot 3\ \text{bits/event} = 0.000320\ \text{cm/event} \quad (30)$$

An event causing that change in length of the spring would be due to a change in force on the spring of:

$$F = k \cdot x \quad (31)$$

$$x = 0.000320\ \text{cm} = 0.000000320\ \text{m} \quad (32)$$

$$k = 2900\ \text{pounds/inch} = 508000\ \text{N/m} \quad (33)$$

$$F = 508000 \cdot 0.000000320 = 0.163\ \text{N} \quad (34)$$

A change in centrifugal force of that magnitude at top speed would be due to a mass loss of:

$$F = m \cdot \omega^2 \cdot r \quad (35)$$

$$m = F/(\omega^2 \cdot r) \quad (36)$$

$$m = 0.163/(85.8^2 \cdot 0.4) \quad (37)$$

$$m = 0.0000553\ \text{kg} = 0.055\ \text{g} \quad (38)$$

Alternately, one can compute the minimum speed at which a mass loss of 1 gram is detectable:

$$F = m \cdot \omega^2 \cdot r \quad (39)$$

$$\omega = \sqrt{\frac{F}{m \cdot r}} \quad (40)$$

$$\omega = \sqrt{\frac{0.163}{0.001 \cdot 0.4}} \tag{41}$$

$$\omega = 20.2 \text{ radians / second} \tag{42}$$

For comparison, the equivalent tangential speed of the sample at the specified radius of 0.4 meters at a top radial speed of 85.8 radians/second is:

$$\frac{85.8 \text{ radians}}{\text{second}} \cdot \frac{1 \text{ revolution}}{2\pi \text{ radians}} \cdot \frac{2\pi \cdot 0.4 \text{ meters}}{1 \text{ revolution}} = 34.3 \frac{\text{meters}}{\text{second}} = 76.8 \frac{\text{miles}}{\text{hour}} \tag{43}$$

And, the equivalent tangential speed of the sample at the minimum speed of 20.2 radians/second necessary to detect a mass loss event of one gram is:

$$\frac{20.1 \text{ radians}}{\text{second}} \cdot \frac{1 \text{ revolution}}{2\pi \text{ radians}} \cdot \frac{2\pi \cdot 0.4 \text{ meters}}{1 \text{ revolution}} = 8.04 \frac{\text{meters}}{\text{second}} = 18.0 \frac{\text{miles}}{\text{hour}} \tag{44}$$

In order to distinguish mass loss events at lower speeds, a less stiff spring can be used; however, this will also decrease the highest speed at which the apparatus can be run before the spring fully compresses. Initial screening experiments can be used to determine the characteristic range of speeds over which mass loss events are expected to occur, and a suitable spring rate can be chosen.

Another practical consideration relating to the primary sensing strategy is the DC voltage range over which the data logger detects changes on any given channel. For example, if the data logger is configured for a range of 0-5 volts, then the DC voltage used to excite the displacement transducer must be carefully matched such that the actual range of displacement (in this case, from 0-1.75 cm) corresponds to a voltage change of 0-5 volts. Hence, the DC voltage used to supply the displacement transducer in order to maximize its resolution:

$$1.75 \text{ cm} / 5 \text{ V} = 2.5 \text{ cm / excitation V} \tag{45}$$

$$\text{excitation V} = 2.5 / (1.75 / 5) = 7.14 \text{ V} \tag{46}$$

The precise excitation voltage can be achieved using DC batteries and a simple voltage-divider circuit.

# Alternate Analysis Strategies

As discussed above, the video camera captures a video record of every particle that leaves the test sample within the field of view. Frame-by-frame analysis of the video recording using, for example, the freely available VirtualDub software package reveals individual mass loss events. Correlating the time of each video frame with the recorded speed of the apparatus results in the speed and accelerations experienced during each mass loss event.

The smallest detectable mass loss event using this method is determined by the resolution of the video camera, distance from the sample and density of the ejecta. In the setup, the field of view at the depth of the sample in the video frame is approximately 33 cm wide by 25 cm high. The on-board DVR records at a resolution of 320x240 pixels. The effective resolution of the on-board video system is therefore:

$$\frac{33 \text{ cm} \cdot 25 \text{ cm}}{320 \text{ pixels} \cdot 240 \text{ pixels}} = 0.0107 \frac{\text{cm}^2}{\text{pixel}^2} \tag{47}$$

or about 1 mm per pixel in either direction.

Assuming ejecta density of 1 gram/cubic centimeter, the video setup is capable of detecting mass loss events three orders of magnitude smaller than the primary sensing strategy, and is not limited to any particular speed range. However, the frame rate of the video must be fast enough to capture mass loss events at a particular speed. The DVR in the setup records at 30 frames per second. If a particle of ejecta travels across half of the vertical video frame to be detectable, that is approximately a distance of 15 cm. The video speed of 30 frames per second means a particle of ejecta has 0.0333 seconds to be captured in a video frame. Therefore, if the particle is traveling at more than 15 cm/0.0333 second = 450 cm/second = 4.5 meters/second = 10 miles/hour, it will not be shown traveling in the video frame. At higher speeds, a mass loss event will only be discernible by the presence of the ejecta particle on the sample in one frame and its absence in an adjacent frame. Other principal drawbacks of the video analysis method include the time involved in frame-by-frame video analysis, and the possibility that an event may be occluded by another event in the video frame.

To augment the video analysis, audio data recorded off-board the apparatus can also be used to detect mass loss events. The smallest mass loss event discernible using this method depends on the rigidity of the surface on which the ejecta impacts, the rigidity of the ejecta itself, the noise produced by the apparatus and other ambient noise. Using a radial protective shield made of 6mm-thick steel around the machine, the system is able to distinguish mass loss events using this method. Applying a high-pass filter to the data (greater than the rotational speed of the machine) helps to reduce noise in the data. Limitations of this method include difficulty in synchronizing the audio data with the start of the machine rotation, the time lag between when ejecta leave the sample and impact the blast shield, inability to distinguish the position from which ejecta leave the sample,

inability to distinguish the sizes of individual particles of ejecta, and confounding of the signal by secondary impacts (ejecta striking the radial wall, then falling to strike again).

# Sample Data

An interesting trend in data obtained using the primary sensing strategy is related to the mass loss from the sample over time. As mass is lost from the sample, the sprung mass decreases and, therefore, the amplitude of the oscillations caused by gravity decreases as the sample rotates around from pointing straight up to pointing straight down. This effect is shown graphically in Figure 11. The region where the amplitude of the oscillations decreases helps to identify the time interval during which the mass is being lost.

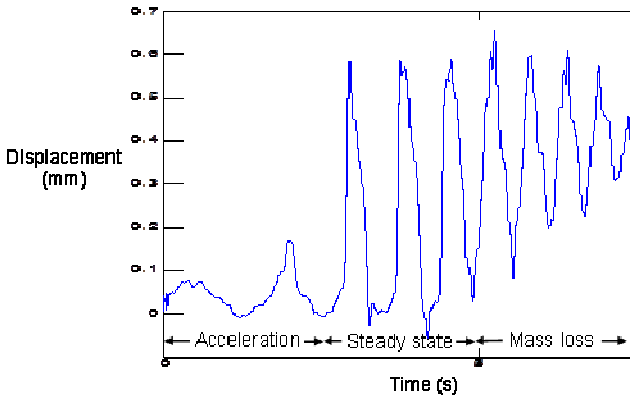


**Figure 11. Sample Data from the Displacement Transducer Showing Change in Amplitude Induced by Mass Loss Events**

Sample data obtained using the video analysis is shown in Table 3. The analysis proceeds from the frame number of a noticeable event, the time corresponding to that video frame, an estimate of the mass of the ejecta based on the size in the video frame, a running total of the accumulated mass loss over time, the computed tangential speed at which each event occurred, and computed force and acceleration experienced by each particle of ejecta. The same data are plotted versus time and versus tangential speed in Figure 12.

The plots in Figure 12 illustrate how most of the mass loss events occur over a narrow critical speed range where enough force is experienced by the ejecta to dislodge them from the test sample. Note that the smallest estimated particle of ejecta is 4.8 grams. Thus, the principle goal for the device, to detect mass loss events on the order of single grams from individual parts spinning at speeds sufficient to achieve centripetal accelerations on the order of hundreds of g's, has been achieved.

**Table 3. Sample Data from Video Analysis**

| frame # | time (s): | mass estimate (g): | accumulated mass loss (g): | speed (mph): | total force (N): | force on chunk (N): | accel. (m/s^2): | accel. (g's): |
|---|---|---|---|---|---|---|---|---|
| 254 | 8.47 | 0 | 0 | | | | | |
| 255 | 8.50 | 38.4 | 38.4 | 24.3 | 1787 | 8.93 | 233 | 23.7 |
| 263 | 8.77 | 4.8 | 43.2 | 24.5 | 1845 | 1.15 | 240 | 24.5 |
| 274 | 9.13 | 4.8 | 48.0 | 24.6 | 1927 | 1.20 | 251 | 25.6 |
| 278 | 9.27 | 4.8 | 52.8 | 24.7 | 1907 | 1.19 | 248 | 25.3 |
| 280 | 9.33 | 76.7 | 129.5 | 24.7 | 1989 | 19.88 | 259 | 26.4 |
| 281 | 9.37 | 9.6 | 139.1 | 24.7 | 1957 | 2.44 | 255 | 26.0 |
| 283 | 9.43 | 14.4 | 153.5 | 24.8 | 1951 | 3.47 | 241 | 24.6 |
| 284 | 9.47 | 38.4 | 191.9 | 24.8 | 1954 | 9.26 | 241 | 24.6 |
| 285 | 9.50 | 19.2 | 211.0 | 24.8 | 1904 | 4.76 | 248 | 25.3 |
| 286 | 9.53 | 76.7 | 287.7 | 24.8 | 1967 | 19.66 | 256 | 26.1 |
| 288 | 9.60 | 9.6 | 297.3 | 24.8 | 1981 | 2.47 | 258 | 26.3 |
| 291 | 9.70 | 38.4 | 335.7 | 24.8 | 1959 | 9.28 | 242 | 24.7 |
| 292 | 9.73 | 48.0 | 383.6 | 24.8 | 1899 | 11.86 | 247 | 25.2 |
| 293 | 9.77 | 9.6 | 399.2 | 24.8 | 1984 | 2.45 | 258 | 26.1 |
| 298 | 9.93 | 4.8 | 398.0 | 24.9 | 1867 | 1.17 | 243 | 24.8 |
| 305 | 10.17 | 4.8 | 402.8 | 24.9 | 1873 | 1.17 | 244 | 24.9 |
| 323 | 10.77 | 4.8 | 407.6 | 25 | 2035 | 1.27 | 265 | 27.0 |
| 327 | 10.90 | 4.8 | 412.4 | 25 | 1888 | 1.18 | 246 | 25.1 |
| 328 | 10.93 | 0.0 | 412.4 | | | | | |
| | 2.47 | 412.4 | 412.4 | 24.8 | 1909 | | 248.6 | 25.3 |
| | Total | Total | Total | Avg. | Avg. | | Avg. | Avg. |

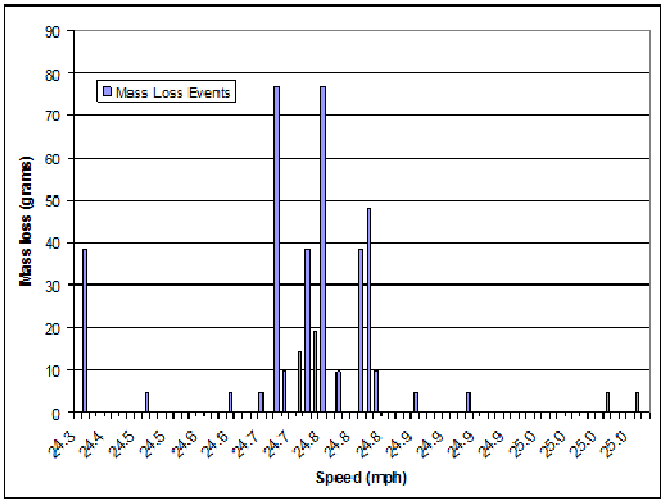


**Figure 12. Mass Loss Events Based on Analysis of Video Data**

Finally, a plot of the off-board audio data for one test is shown in Figure 13. A high-pass filter of 4,015 Hz was applied to the data using the freely available Audacity software package. Individual impacts of ejecta against the steel blast shield are clearly visible (highlighted with red arrows in Figure 13) in the data and correlate with the times of mass loss events recorded using the video analysis method.

# Conclusion

The development of an apparatus and associated sensing strategies and analysis methods as reported in this paper allow test engineers to study the speeds, accelerations and forces at potentially dangerous mass loss events that occur on rotational machinery. While the video analysis produced the most useful data for the proprietary tests conducted,

given another situation, one of the other analysis strategies described may well produce more relevant data. The experimental apparatus has also been used to study the mechanics at the interface between various ejecta materials and different substrates, as the apparatus allows for experiments to be conducted at high acceleration levels in controlled laboratory conditions. Future work should include the application of the apparatus and analysis strategies to additional physical phenomena at high acceleration levels.

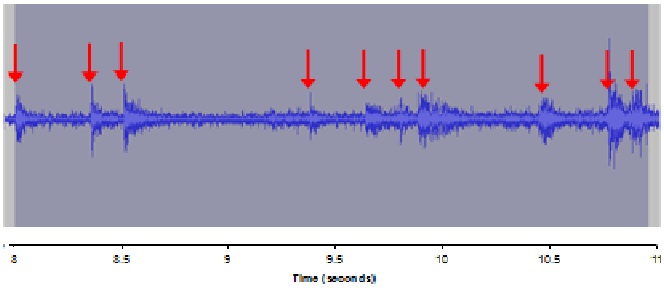


**Figure 13. Processed Audio Signal from Off-Board Recording**

# References


[1] Bureau of Labor Statistics. (2006). Fatal occupational injuries by primary and secondary source of injury by major private industry sector. *Technical Report.* United States Department of Labor, pp. 1–17. Retrieved February 11, 2013, from http://www.bls.gov/iif/oshwc/cfoi/cftb0208.pdf.

[2] National Highway Traffic Safety Administration. (2007). Research Report to Congress on Tire Aging. *Technical Report.* NHTSA. Washington, DC.

[3] Pegula S. M. (2004). Fatal Occupational Injuries Involving Helicopters, 1995-2002. *Technical Report.* Bureau of Labor Statistics. Retrieved February 11, 2013, from http://www.bls.gov/opub/cwc/old/sh20041022ar01p1.asp.

[4] Takeuchi K. (1997) Aircraft Accident Investigation Report: Garuda Indonesia, Douglas DC-10-30, PK-GIE Fukuoda Airport. Aircraft Accident Investigation Commission, Technical Report, Tokyo, Japan.

[5] Nordmann R. (1994). Identification techniques in rotordynamics. Diagnostics of Rotating Machines in Power Plants: *Proceedings of the CISM/IFToMM Symposium*, October 27-29, 1993, Udine, Italy, Springer, p. 1.

[6] Pahl G., Beitz W., Wallace K., & Blessing, L. (2007). *Engineering Design: A Systematic Approach*, Springer-Verlag London Limited, London.

[7] Kocabas H. (2009). Gripper design with spherical parallelogram mechanism. *Journal of Mechanical Design*, 131 (7), .

[8] Arakelian V., & Guégan S. (2008). Design and prototyping of a partially decoupled 4-DOF 3T1R parallel manipulator with high-load carrying capacity. *Journal of Mechanical Design*, 130 (12), pp. 122301–122303.

[9] Zoppi M., Sieklicki W., & Molfino R. (2008). Design of a Microrobotic Wrist for Needle Laparoscopic Surgery. *Journal of Mechanical Design*, 130 (10), p. 102306.

[10] Lin C. (2002). Finite element analysis of a computer hard disk drive under shock. *Journal of Mechanical Design*, 124 (1), pp. 121–125.

[11] Yoshikawa K. (1999). Embedded flash memories-technology assessment and future. *VLSI Technology, Systems, and Applications, 1999. International Symposium on*, IEEE, (pp. 183–186).


# Biographies


**JONATHAN R. A. MAIER** is a lecturer in General Engineering at Clemson University. He received his BS from Georgia Tech and his MS and PHD at Clemson University. His research is centered on affordance based design, establishing it as both an explicative theory for design and evolving design methods based on the theory. Dr. Maier may be reached at jmaier@clemson.edu.

**M. LAINE MEARS** is an Associate Professor of Automotive Engineering at Clemson University. He received his BS from Virginia Tech and his MS and PHD from Georgia Tech. His research interests include manufacturing process control. He is an NSF CAREER award recipient and his work has been funded by the US Army, DOE, NIST, and several automotive industry corporations. Dr. Mears may be reached at mears@clemson.edu.

**JOSHUA D. SUMMERS** is a Professor of Mechanical Engineering and a College IDEaS Named Professor at Clemson University. He received his BS and MS degrees from the University of Missouri and his PHD from Arizona State University. His research interests are centered on understanding the design process in order to develop new design enabling tools and methods. He may be reached at jsummer@clemson.edu.